HIGH SPEED OPTICAL TOMOGRAPHY FOR FLOW VISUALIZATION

Ray Snyder and Lambertus Hesselink

Department of Aeronautics/Astronautics
and Electrical Engineering
377 Durand
Stanford University
Stanford California 94305-2186

ABSTRACT

A novel optical architecture (based on holographic optical elements) for making high speed tomographic measurements is presented. The system is designed for making density or species concentration measurements in a non-steady fluid or combusting flow. Performance evaluations of the optical system are discussed and a test phase object has been successfully reconstructed using this optical arrangement.

INTRODUCTION

Optical computer assisted tomographic (OCAT) reconstruction of a three-dimensional unsteady object requires simultaneous acquisition of many line-of-sight measurements (projections). A projection represents an integrated measurement of absorption or index-of-refraction along a ray path. To acquire one projection a source, often a laser, is used in conjunction with beam steering and recording elements; all necessary projections can be obtained by either rotating the object, by rotating the data acquisition apparatus or alternatively by replicating the system required for making one projection. These approaches have been investigated by us and others for the purpose of making, for instance, measurements of the flow around a revolving helicopter rotorblade[1] or time averaged measurements of complicated turbulent flows[2]. Byer and coworkers have proposed OCAT for monitoring

of atmospheric pollutants; they have devised a data acquisition system which, at least in principle, could provide time-resolved measurements (at a rate of approximately 1 millisecond per cross section), but at present has only been used to make measurements of static objects in their configuration. A rotating mirror is located at the center of a ring of detectors and isotropic scatterers. This system measures absorption in a plane only (but could possibly be extended to make volumetric measurements) and the signal-to-noise ratio is severely limited by speckle noise when using a laser light source[3]. Sweeney and Vest[4] used holographic interferometry for making temperature measurements above a heated plate, but their system was not designed for making time-dependent measurements either.

In this paper we discuss a novel optical data acquisition system which is simple in its layout, involves only two rotating parts and incorporates holographic optical elements (HOE) for beam steering and beam shaping. The system proposed and investigated here is capable of recording high resolution images (10,000 - 100,000 pixels per cross section) at a rate of 500-1000 cross sections per second. The performance of the HOEs is investigated in terms of efficiency, resolving power and signal-to-noise ratio. To investigate the validity and usefulness of the concept, a test phase object consisting of a glass rod placed in a container filled with index-matching fluid is reconstructed from a series of interferograms which have been made with the new optical system.

OPTICAL DATA ACQUISITION ARCHITECTURE

To reconstruct a complex three-dimensional object from its projections it is usually necessary to obtain projections spaced at regular angular intervals over a 180° arc. Sometimes it is possible to reconstruct an object from a limited number of projections[1], but this is only useful for a restricted class of problems. Therefore we will concentrate on optical data acquisition systems which allow full viewing of the object over a 180° arc.

Schematically, the experimental configuration is indicated in figure 1. An argon

pumped dye laser beam is incident on a beam splitter. The object wave is expanded, collimated and directed by a combination of a spatial filter and a holographic optical element (HOE1). The expanded beam probes the test object and either the absorption coefficient or the optical pathlength is measured along the raypaths. The transmitted object beam is then imaged by element HOE2 onto the image plane (camera). At this location the intensity of the transmitted beam is measured or phase information is recorded by heterodyne detection with a reference wave. Multiple views are obtained by using two synchronized spinning mirrors, M1 and M2. For the test configuration described here only two HOEs are used and the mirrors M1 and M2 are stationary; to obtain multiple views for this test case the glass rod, which is immersed in an index matching fluid, is rotated about the cylinder axis. The objective of this experiment is to test the usefulness of the HOEs for optical tomographic data acquisition and to investigate the pertinent properties of the elements, such as diffraction efficiency, aberration tolerances and ease of fabrication.

As an example we discuss the design requirements for the different components, assuming that 100 projections are taken per millisecond and each projection contains 100 rays or bins. The object cross-section is 25 square centimeters and the probe beam diameter is 5 centimeters so that the area of overlap of all projections covers the complete cross-section of the flowfield. These requirements imply that the mirrors should be spinning at a rate of 30,000 rpm (assuming two mirror faces per scanner in order to minimize the offset from the spinning axis) and a 100 element linear detector array should be read out at a rate of 10 Megabytes per second assuming 8 bits of accuracy. If film is used as a recording medium the framing speed should be 100,000 frames per second. These specifications can be achieved with presently available commercial instrumentation. However, if the time requirement is relaxed to obtaining 100 projections every 2 milliseconds (500 Hz) the implementation of the data acquisition system becomes substantially simpler; we have adopted the latter requirements during the initial phase of the work, but intend to find ways to improve the time resolution at a later stage after we have obtained experience

with a less demanding system.

METHOD

Although higher efficiency HOEs could be obtained in dichromated gelatin emulsions, we have selected conventional silver halide film (Agfa 8E75HD-NAH holographic plates) for its ease of use. The holograms are developed in the catechol developer described by Cooke and Ward[5]; no fixer is used. The developed plates are bleached in GP432[6] for increased efficiency.

The holograms are constructed in a geometry identical to that for which they are to be used; a converging beam is interfered with a collimated beam at an angle of 33° from opposing, representative of the geometry for an average element in a multi-projection system. Since the beams enter the plate from opposite sides, a reflection hologram is formed. The converging beam is focused to a spot 47 centimeters from the plate, so that the created holograms have a focal length of 47 centimeters. The collimated beam to converging beam intensity ratio is 2. The resulting HOEs are reflecting, focusing lenses at the construction wavelength of 589 μm in and near the construction geometry. 10% diffraction efficiency (diffracted intensity in desired component / incident intensity) is easily obtained for an aperture greater than 3 centimeters in diameter. Substantially higher efficiency (approximately 24%) has been achieved with this process in other configurations in our laboratory.

Two HOEs are used in the experiment as shown in figure 1. To evaluate the spatial resolving power of the HOEs, a standard Air Force test target is placed at the object position and imaged onto the image plane by the second HOE at 2.4× magnification. The result is shown in figure 2; resolution better than 10 lines per millimeter is obtained. Illumination falls off in the corners of the image due to nonuniformity of the illuminating beam but it is uniform in the central region and no distortions are apparent. The potential

for achieving resolution greater than 200 pixels per projection is clearly evident.

To obtain interferograms, a reference beam was split off from the laser before the spatial filter shown in figure 1 and independently filtered, directed and focused using conventional optics. The reference beam and the object beam are recombined at the image plane. The fringes resulting are viewed in the image plane corresponding to the object. The resulting fringe patterns show a high signal-to-noise ratio.

For the tomographic experiment, a 2.2 millimeter cylindrical pyrex rod is used as the object. The rod, with a nominal index of 1.474, is immersed in index matching fluid with an index of 1.47. The magnification in the image plane is 3.5×; the imaging greatly reduces the distortion caused by raybending as the rays passing through the object encounter index of refraction gradients[7]. A sample interferogram is shown in figure 3. Ten interferograms are recorded, each corresponding to one angular position of the rod. The rod was rotated 36° between images so that an arc of 360° is viewed.

The images are digitized with a PDS model 1010A scanner with a pixel size of 50 μm square to form a 512×512 array. The data base is reduced by extracting a 128 pixel high by 360 pixel wide window from each image as shown in figure 3. Since the rod is very nearly vertical and the properties of the rod depend only slightly on its axial coordinate as demonstrated in figure 3, the fringes are periodic along the z coordinate. It is seen that any pixel in the windowed data is reproduced periodically along a vertical axis. The period is one seventh of the window height. A one-dimensional Fourier transform of a column of data yields a spectrum from which the phase offset of the fringes can be determined across the width of the window. Figure 4 shows the averaged magnitudes for the whole window of the vertical frequency components of one view. Note that aside from the large D.C. component, seven cycles per window is the major energy containing component, the one corresponding to the fundamental spacing of the fringes; lower energy harmonics are also present. If the phase of the seventh component is extracted for each column and

plotted versus the width of the window, the result is as shown in figure 5. This phase plot corresponds to the relative spatial offset of the fringes in the interferogram.

The phase information is unraveled by addition and subtraction of integer multiples of π at discontinuities in figure 5. The correct multiple was selected manually by comparing figures 3 and 5; the correct phase plot is expected to be identical in form to the trace of a single fringe in figure 3. The background phase variation is eliminated by fitting a third order polynomial to the background phase at either side of the rod in each interferogram, and then subtracting the function from the whole field. The result is as shown in figure 6, which constitutes the reduced optical pathlength measurements of one projection.

The ten single projections are averaged with their complementary projections, 180° away, to yield five projections spaced at 36° to cover a 180° arc of view. These five projections are aligned to the same origin, or axis of rotation, by placing the axis at the centroid [where values less than $-\frac{\pi}{2}$ are weighted uniformly and values greater than $-\frac{\pi}{2}$ receive no weight] of the image and filling in at the sides with zeros. By linear interpolation the five projections are extended to one hundred projections at 1.8° spacing as shown in figure 7. Convolution backprojection[8] with a Shepp-Logan filter[9] is used for reconstruction. When median filtering with a 3×3 window is performed (to remove spikes caused by reconstruction of sharp gradients) the results are as shown in figures 8 and 9 on a 128×128 grid. Figure 10 shows a cross section through the center of the reconstruction*. After the tomographic measurements had been completed, the rod was cut and polished so the cross section could be examined. A photograph of the index of refraction field through a 6 millimeter thick section of the rod is shown in figure 11. Note the spiral pattern which is revealed by incandescent light. The hole in the center is evident and the index of refraction is clearly non-uniform in the cross section, consistent with the tomographic results.

* Note that the dip in the middle of the graph indicates a hole in the center of the rod which was filled with fluid. The index in the hole is slightly lower than the index of the external fluid; this is probably becaused some cleaning solvent, which could not be removed, is mixed in with the index matching fluid. It is also possible that the dip is too low because of the reconstruction scheme used, but this could not be verified.

CONCLUSIONS

Although HOEs have been used to visualize the flow inside a circular cylinder[10], this paper discusses the first application of HOEs for interferometry and tomography of fluid flows. The results indicate that very good data can be obtained with the optical system described here; the signal-to-noise ratio is high and the resolution of the reconstruction can be at least 200×200 pixels. A comparison between the tomographic results shown in figure 9 and the photograph of the cross section in figure 11 shows that the tomographic reconstruction reveals much of the structure of the index-of-refraction present in the rod. In particular the hole and very small index-of-refraction variations are recovered as is the spiral structure of the rod.

Presently an effort is underway in our laboratory to implement the full optical tomographic system; this apparatus will be used to investigate a time-varying, three-dimensional, combusting flow.

ACKNOWLEDGEMENTS

This work is supported by NASA grants NCC-188 and NCA2-OR745-306. Ray Kostuk's assistance with the fabrication of the HOEs is gratefully acknowledged.

REFERENCES

[1] R. Snyder and L. Hesselink, "Optical Tomography for Flow Visualization of the Density Field Around a Revolving Helicopter Rotor Blade," *Applied Optics*, Vol 23, Sept. 1984.

[2] R. J. Santoro, H. G. Semerjian, P. J. Emmerman and R. Goulard, *AIAA*, Vol 80, 1541, 1980.

[3] K. Bennet and R. L. Byer, "Optical Tomography: Experimental Verification of Noise Theory," *Optics Letters* Vol. 9, 1984.

[4] D. W. Sweeney and C. M. Vest, *International Journal of Heat and Mass Transfer*, Vol 17, 1443, 1974.

[5] D. J. Cooke and A. A. Ward, "Reflection-hologram processing for high efficiency in silver-halide emulsions," *Applied Optics*, Vol 23, No. 6, 934-941, March 1984.

[6] Agfa-Gevaert, Holography Newsletter 1, Oct. 1979.

[7] C. M. Vest, "Interferometry of strongly refracting phase objects," *Applied Optics*, Vol. 14, No 7, 1601-1606, July 1975.

[8] G. N. Ramachandran and A. V. Lakshminarayanan, *Proc. Natl. Acad. Sci. U.S.*, Vol. 68, No. 9, 2236-2240, 1971.

[9] L. A. Shepp and B. F. Logan, *IEEE Trans. NS*, Vol. 21, 21-43, 1974.

[10] L. Hesselink, M. Richmand and W. C. Reynolds, "Holographic Optical Element for Flow Visualization Inside a Circular Cylinder," submitted to Appled Optics.

FIGURE 1: Schematic of the experimental configuration. For the tests described, only the beam path shown is employed. The coordinates shown are fixed to the rod. The rod is rotated to obtain projections at angles measured relative to the beam as shown.

FIGURE 2: Image of Air Force test pattern. Smallest visible pattern corresponds to a resolution of at least 10 lines per millimeter in the object.

FIGURE 3: Interferogram for 144° projection. The region outlined by the box is the data window for the projections. Note the periodic structure parallel to the axis of the rod.

FIGURE 4: Spectral energy density averaged over the whole data window of one projection (144°). The seventh component is clearly prominent, with some energy in the 15th component second harmonic).

FIGURE 5: Phase offset of the fringes versus the horizontal component in one projection (144°). Discontinuities occur as the phase exceeds $\frac{\pi}{2}$ or $-\frac{\pi}{2}$.

FIGURE 6: Unraveled phase offset for one projection (144°). The phase wraparound has been removed to make the projection continuous.

FIGURE 7: Interpolated projections. The complete reduced data base is shown inverted for easier viewing.

FIGURE 8: Reconstruction of the index of refraction in the rod.

FIGURE 9: Reconstruction of the index of refraction in the rod. Lighter values correspond to a higher index of refraction. Note the asymmetry and the hole in the center.

FIGURE 10: Cross section through center of the reconstruction. Radial structure is shown as well as hole in the center of the rod.

FIGURE 11: Transmittance photograph of a 6 millimeter long slice of the rod. Note the correspondence with the results of the reconstruction in figure 9. The edge of the rod was chipped as it was being cut.

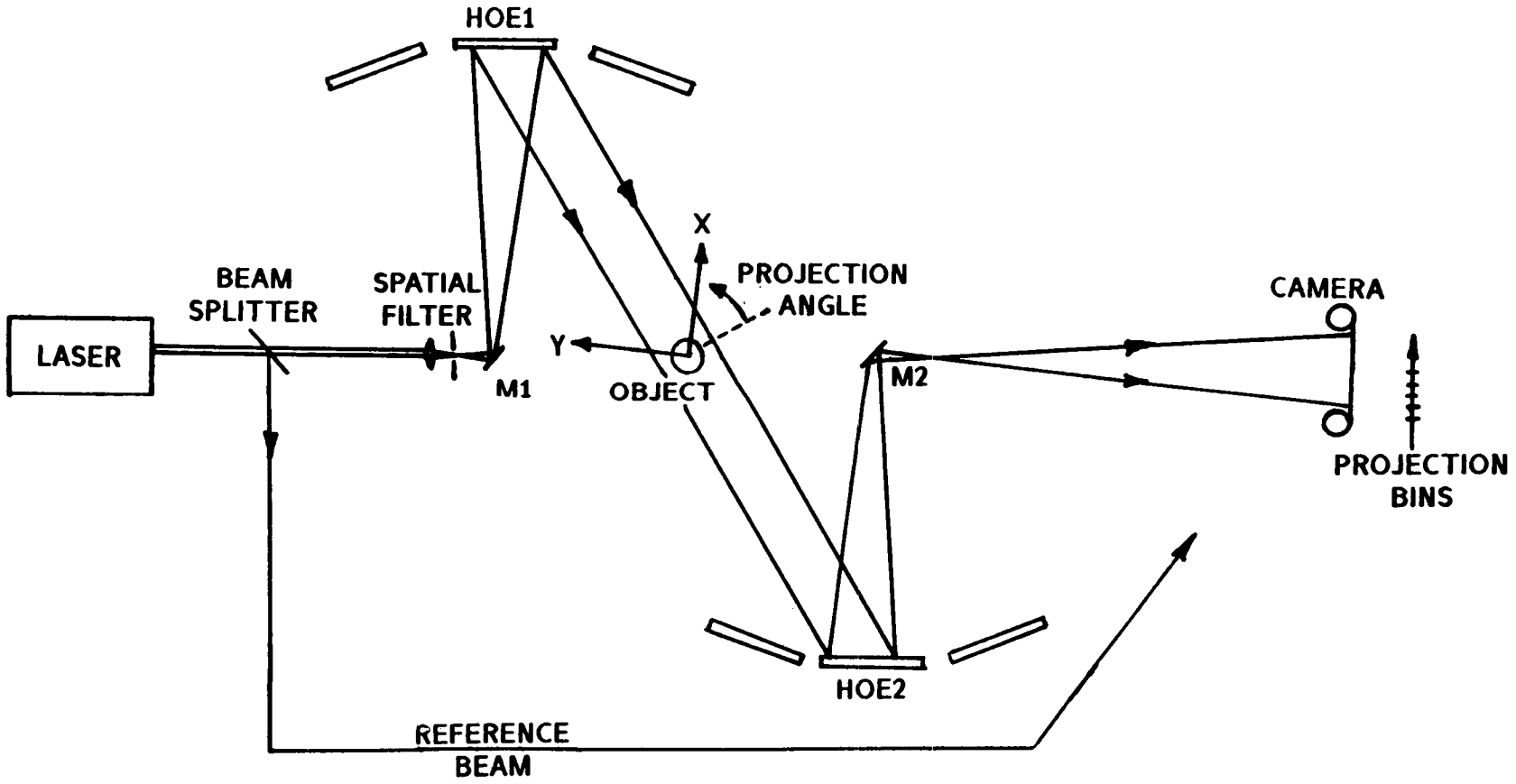
HOE1
X
PROJECTION
ANGLE
BEAM
SPLITTER
SPATIAL
FILTER
LASER
Y
M1
OBJECT
M2
CAMERA
PROJECTION
BINS
HOE2
REFERENCE
BEAM

Fig. 1

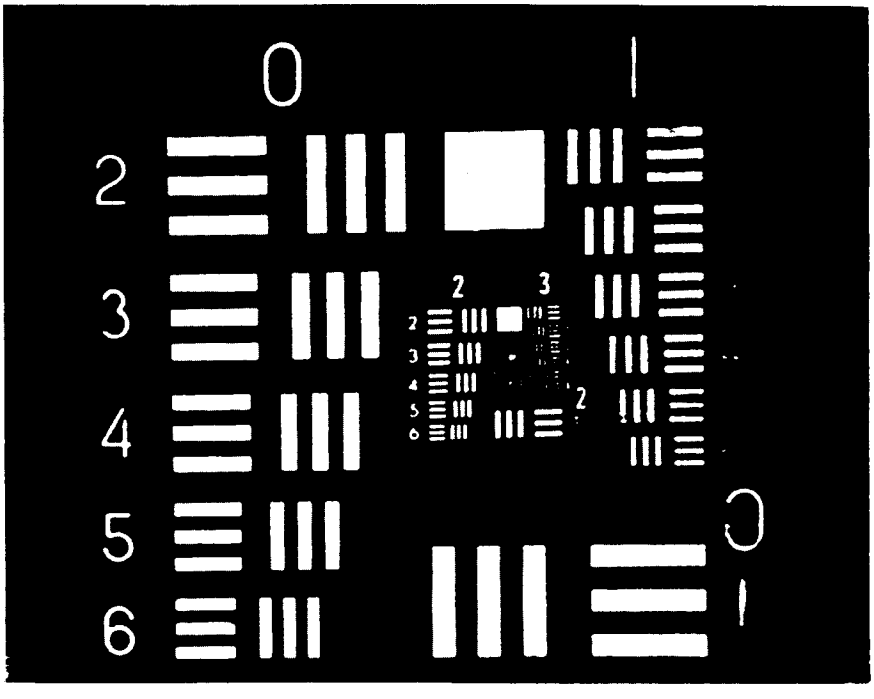

Fig. 2

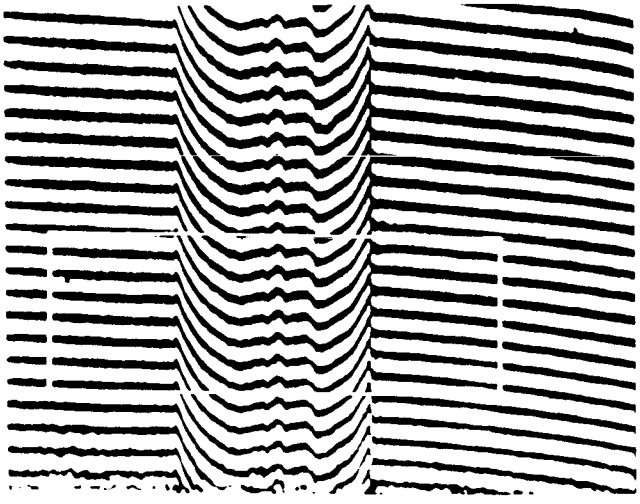

Fig. 3

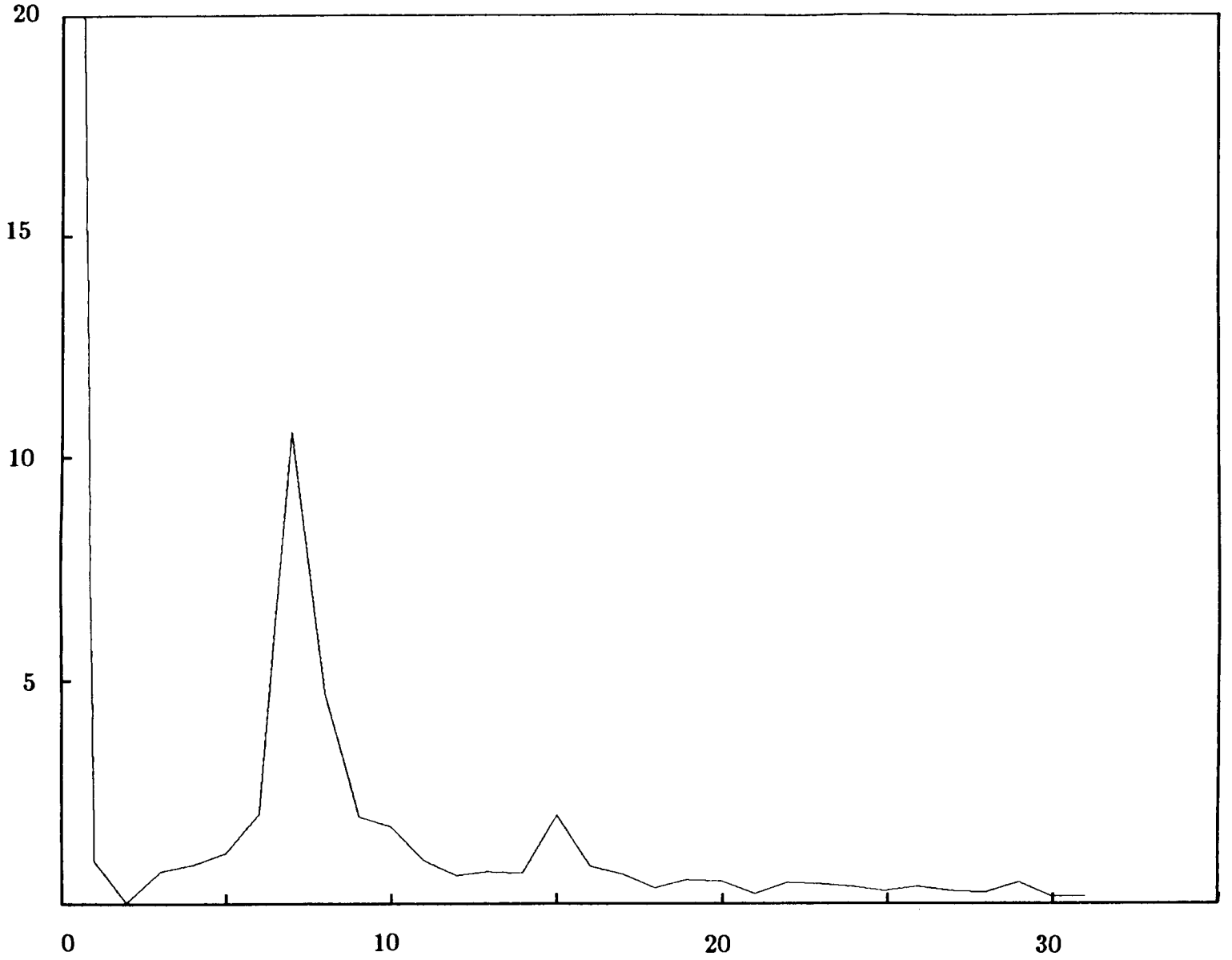
20
15
10
5
0
10
20
30
PERCENT OF TOTAL SPECTRAL ENERGY
FREQUENCY COMPONENT (CYCLES IN WINDOW)

Fig. 4

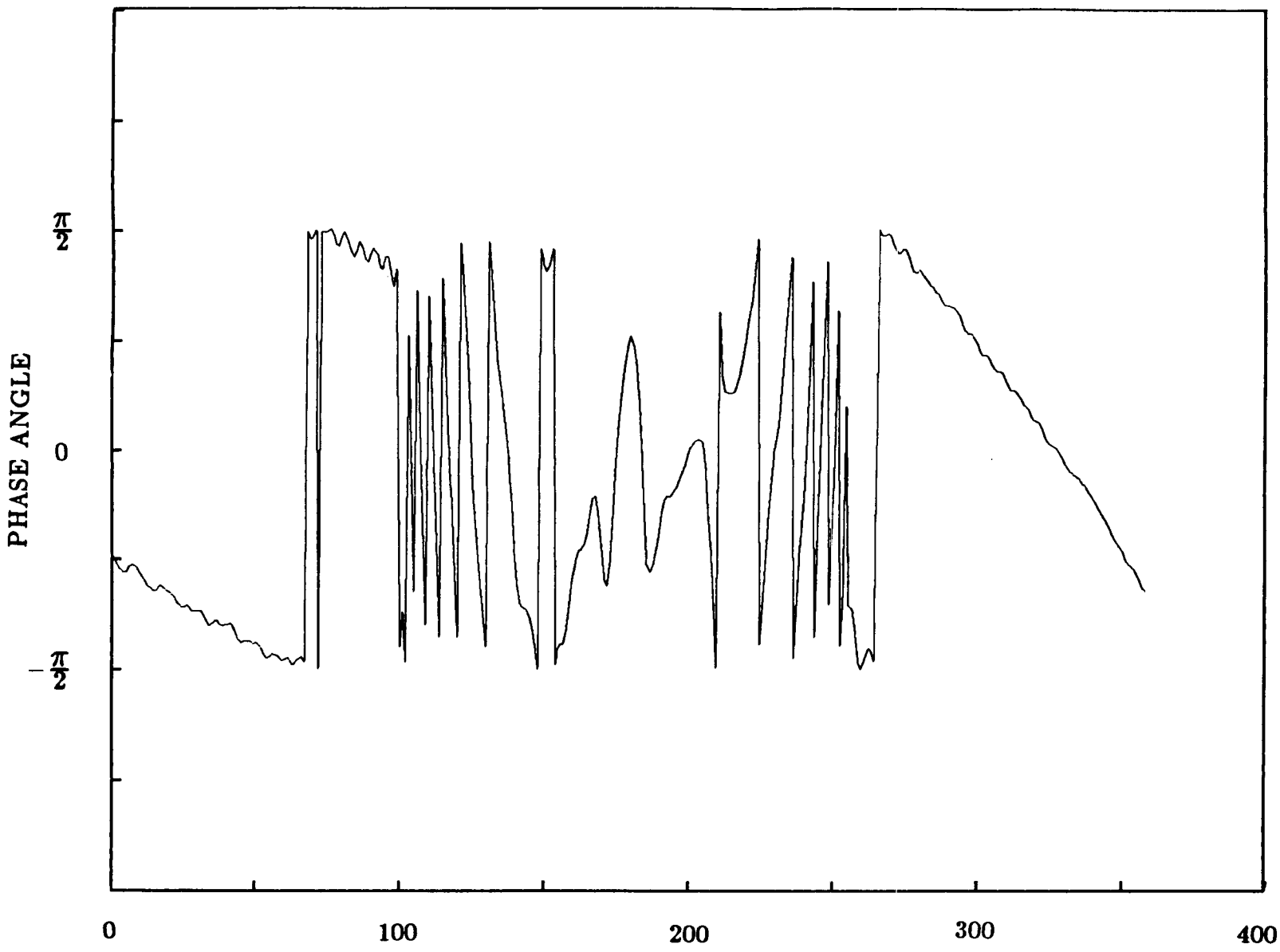

Fig. 5

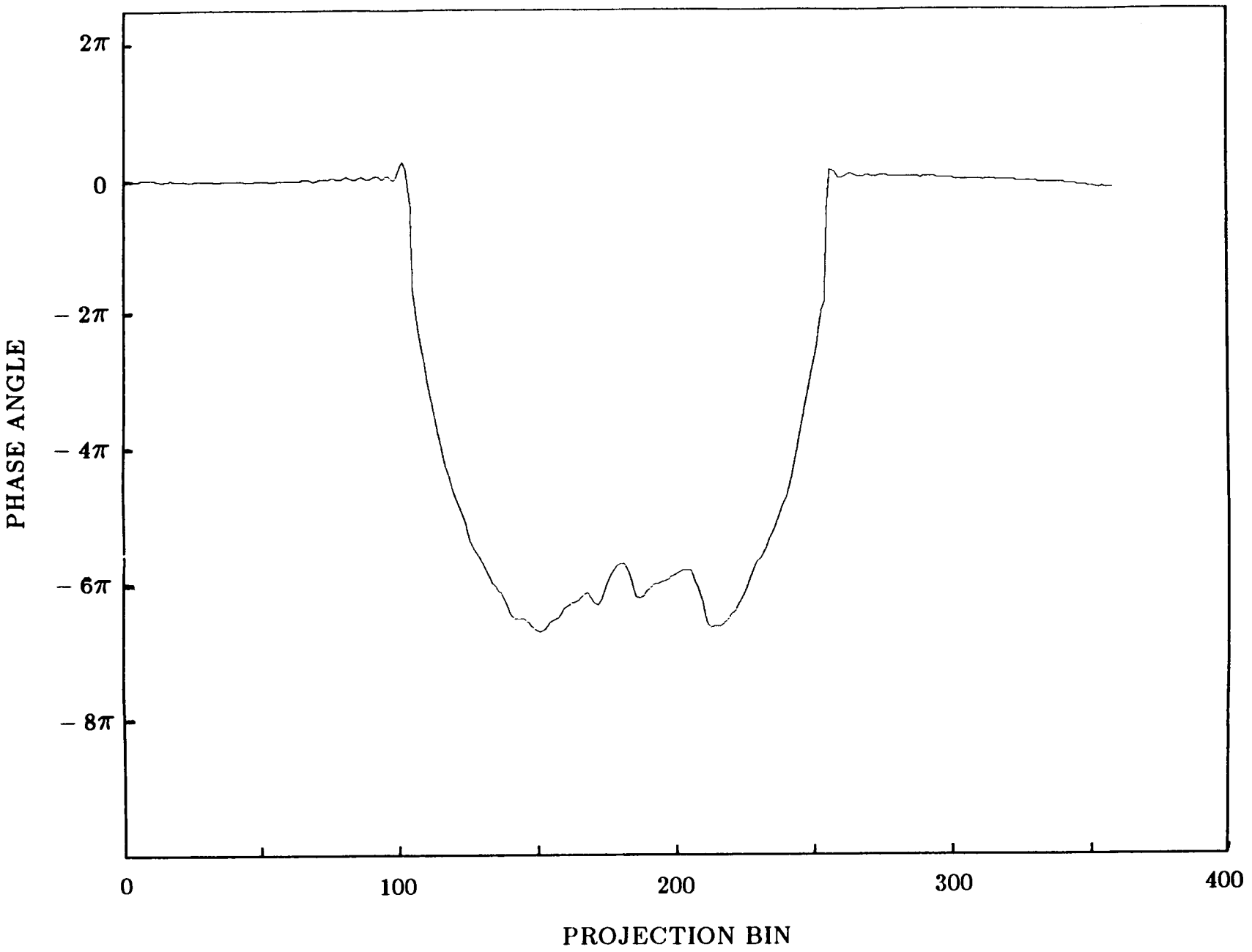

Fig. 6

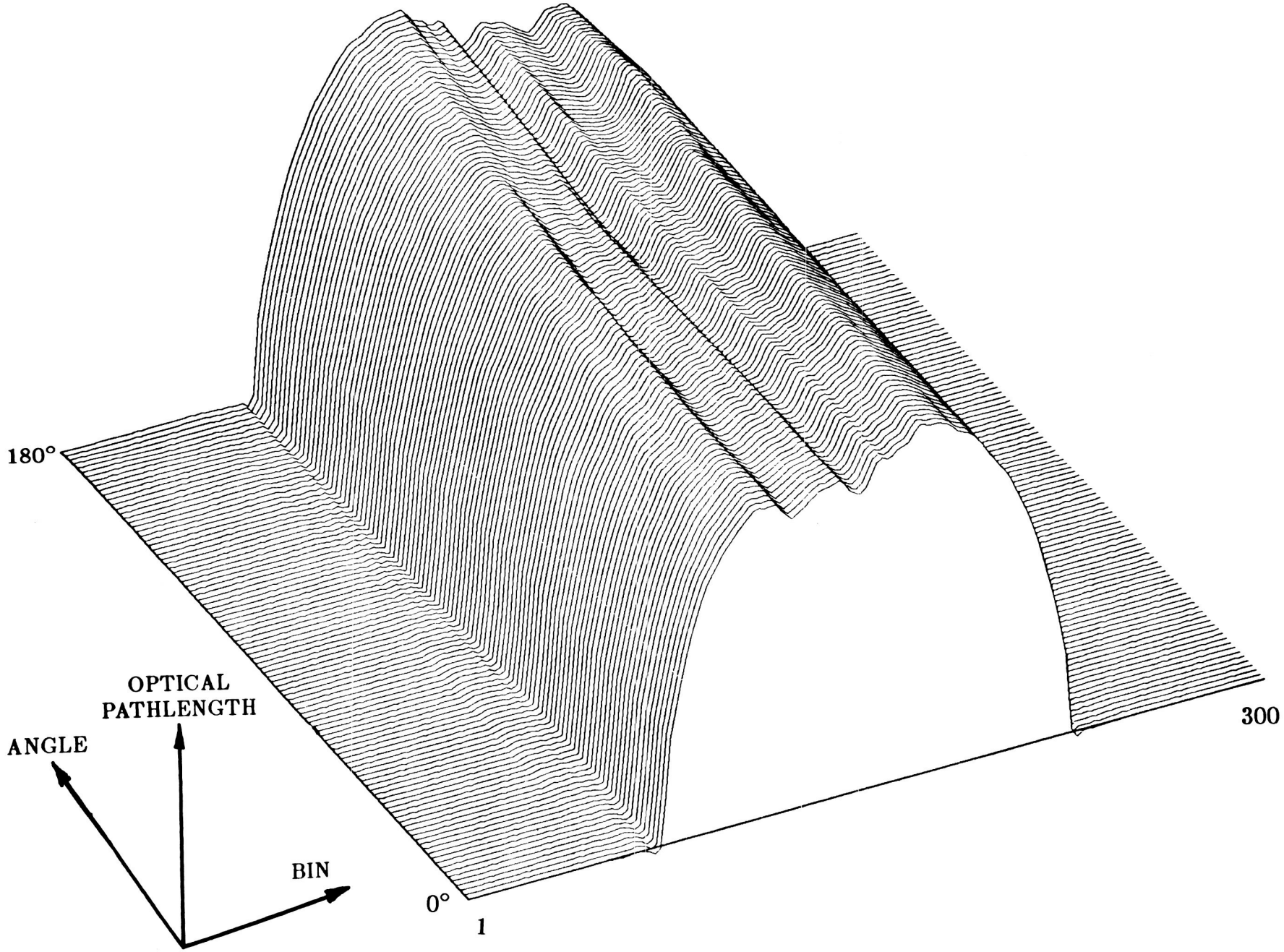

Fig. 7

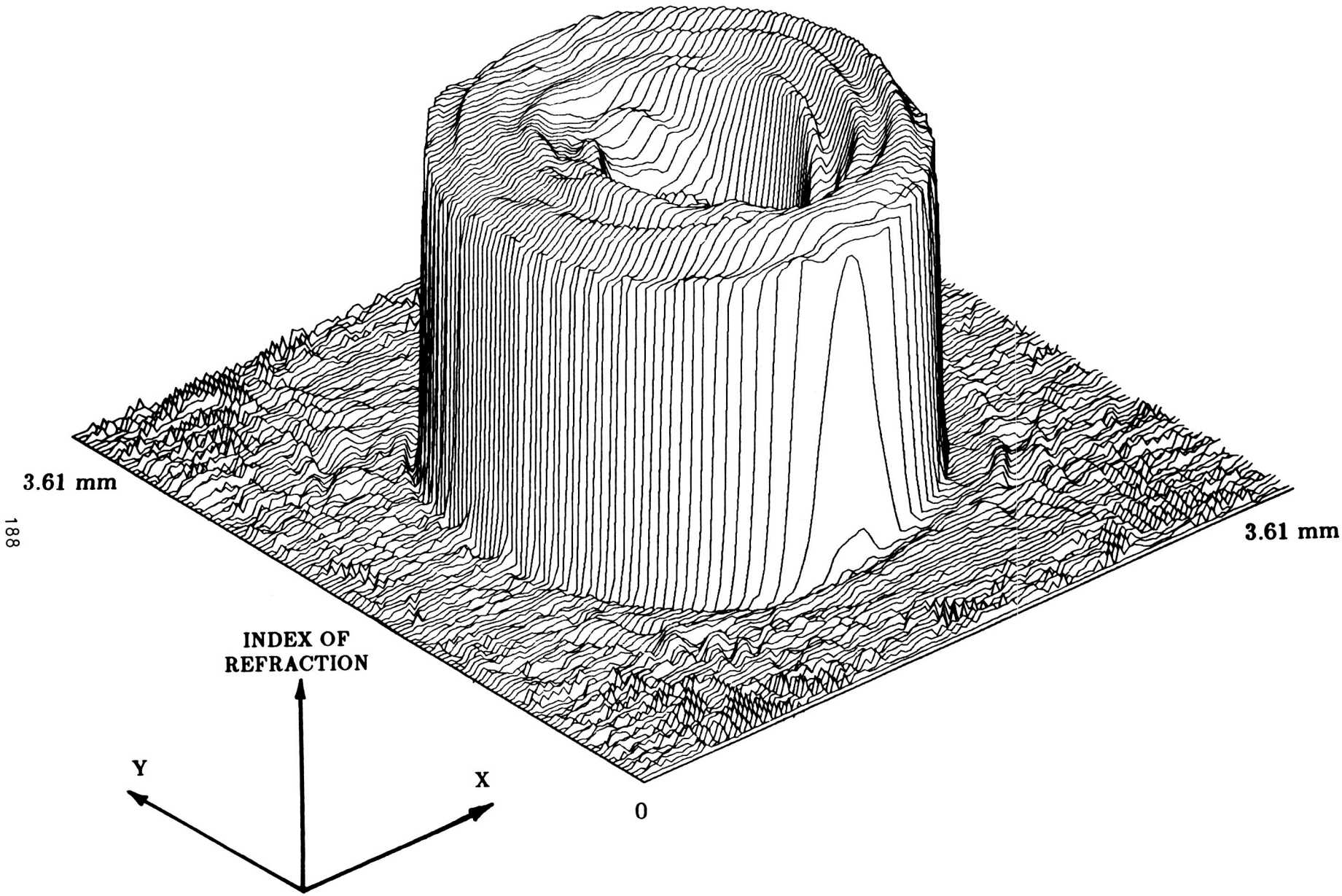

Fig. 8

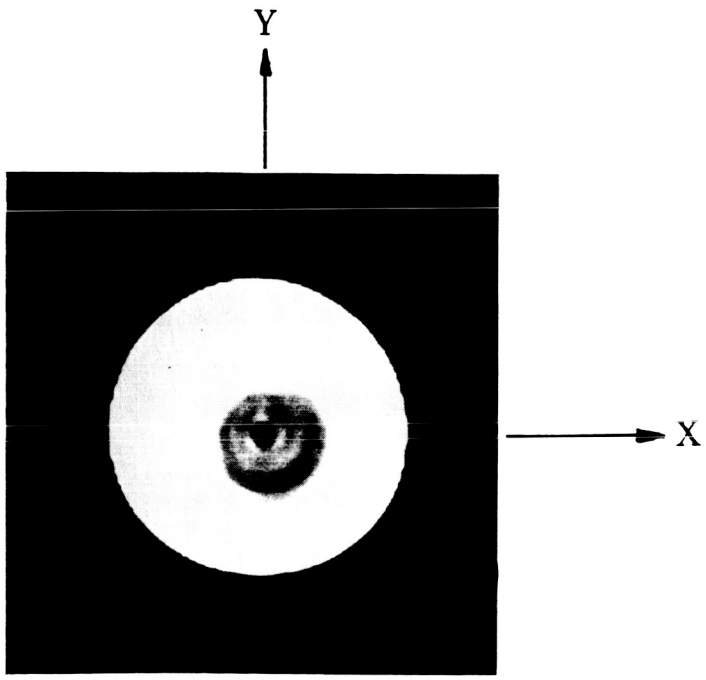

Fig. 9

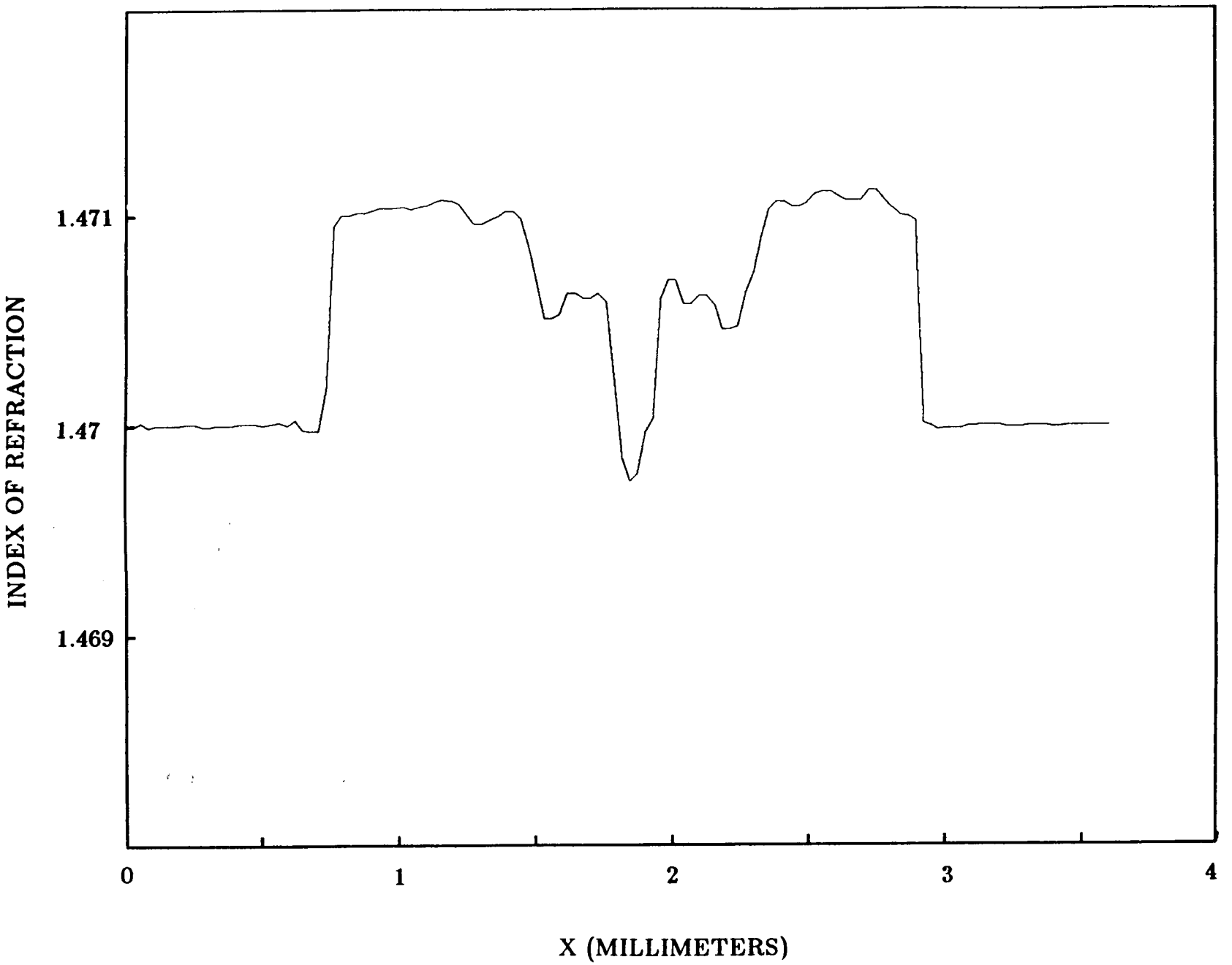

Fig. 10

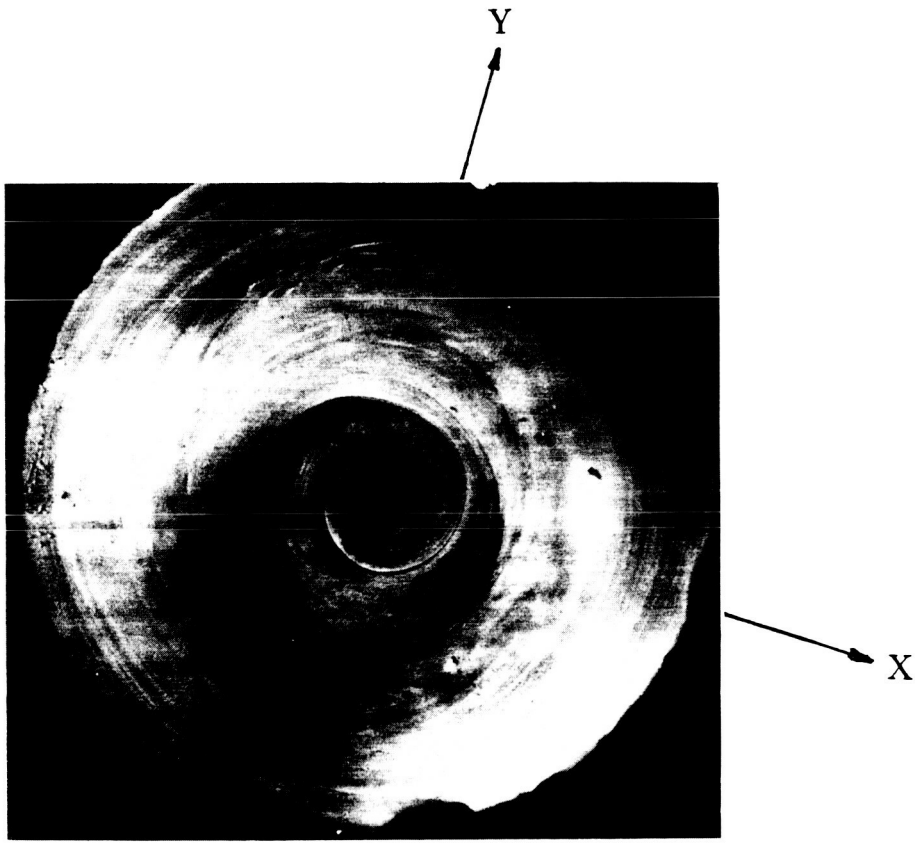

Fig. 11